

Rearrangement of Host Layers upon the Insertion of Organic Cations: Synthesis and Structure of $(\text{CH}_3\text{NH}_3)\text{MnTe}_2$

Joonyeong Kim,[†] Song-Ho Byeon,[‡] and Timothy Hughbanks^{*,†}

Department of Chemistry,
Texas A&M University, P.O. Box 30012,
College Station, Texas 77842-3012, and College of
Environment and Applied Chemistry, Kyung Hee
University, Kyung Ki 449-701, Republic of Korea

Received June 5, 2001

Revised Manuscript Received November 15, 2001

Organic–inorganic hybrid materials offer significant scientific and technological opportunities by combining attractive features of both kinds of compounds within a single material. Potential applications are found in nonlinear optical (NLO) devices, molecule-based magnets, and superconductors.^{1–5} Hybrid materials are often formed by the intercalation of organic species between the inorganic layers in compounds such as MPS_3 ($\text{M} = \text{Fe, Co, Mn, Cd}$), MOCl ($\text{M} = \text{Fe, V, Ti, Cr}$), MQ_2 ($\text{M} = \text{transition metal, Q} = \text{S, Se, Te}$), or MO_3 ($\text{M} = \text{Mo, W}$).^{3,4,6–14} Intercalation usually proceeds with preservation of the host layer structure, with exceptions occurring when intercalation is concomitant with a host–guest redox reaction.¹⁵ Sometimes changes in physical properties are observed due to the incorporated organic species.^{16,17}

Recently, Clement and co-workers reported the synthesis of an organic–inorganic hybrid NLO nanocomposite made by cation exchange of a noncentrosymmetric chromophore, 4-[2(4-dimethylaminophenyl)ethenyl]-

1-methylpyridinium (DAMS^+) into MPS_3 ($\text{M} = \text{Mn, Cd}$).^{3,4} It was concluded that spontaneous poling of DAMS^+ is responsible for an enhanced second-harmonic generating efficiency for these materials. Nevertheless, the reason for spontaneous polarization of DAMS^+ is unclear since the environment between the MPS_3 ($\text{M} = \text{Mn, Cd}$) slabs is symmetrical.

We are interested in evaluating the polar layered compound, LiMnTe_2 , as a potential host for the synthesis of NLO hybrid materials.¹⁸ $[\text{MnTe}_2^-]$ layers in LiMnTe_2 consist of three-corner-shared MnTe_4 tetrahedra; half of the Te atoms (Te2) are bound to three manganese atoms and half (Te1) are bound to only one so that all the Mn–Te1 vectors point in the same direction. Li cations occupy interstices between the layers. The intralayer environment in LiMnTe_2 is noncentrosymmetric and may offer an opportunity of orienting organic dipoles. Here, we report an unusual room-temperature rearrangement of hexagonal host layers upon the exchange of Li^+ with CH_3NH_3^+ ions to produce tetragonal nonpolar layers in the product, $(\text{CH}_3\text{NH}_3)\text{MnTe}_2$.

All experimental operations were carried out under an inert gas atmosphere. LiMnTe_2 was prepared by loading stoichiometric proportions of elemental starting materials in a sealed Nb tube as previously described.¹⁸ NH_4Cl (99.99%, Aldrich) and $\text{CH}_3\text{NH}_3\text{Cl}$ (99%, Aldrich) were purchased and recrystallized from dried acetone several times and dried under vacuum before use. Methanol was dried over sodium methoxide and distilled under N_2 before use. LiMnTe_2 (0.317 g, 1.0 mmol) and $\text{CH}_3\text{NH}_3\text{Cl}$ (0.101 g, 1.5 mmol) were mixed in methanol (ca. 10 mL), sealed in a borosilicate ampule, and stirred for 5 days. Dark brown product was repeatedly washed in dried methanol, separated by centrifuging, and dried under vacuum. The Guinier X-ray powder pattern indicated that product contained a new phase and MnTe_2 (pyrite type) as a minor product. Diffraction data for the new phase were indexed on a tetragonal cell with $a = 4.5524(4)$ Å, $c = 17.029(3)$ Å, and $V = 352.92(7)$ Å³. The cell parameters and peak intensities for the new phase bore some similarity to those of AMnTe_2 ($\text{A} = \text{K, Rb, Cs}$).¹⁹ The c axis of the new phase is about 2.12 Å longer than that of KMnTe_2 , consistent with the size difference between CH_3NH_3^+ and K^+ .^{20,21} The IR spectrum of the product (Mattson Research Series FTIR) exhibited CH and NH stretching bands at 2960 and 3300 cm^{–1}, respectively.²² Atomic absorption measurements (AA, Varian Spectra AA 250 plus) and wavelength-dispersive X-ray spectrometry (WDS, Cameca SX 50) gave $\text{Mn:Te} = 0.99(3):2$ and no other element heavier than Na. AA data revealed that Mn and Te are

- * To whom correspondence should be addressed. Tel.: (979)845-0215. Fax: (979)847-8860. E-mail: trh@mail.chem.tamu.edu.
- † Texas A&M University.
- ‡ Kyung Hee University.
- (1) Bailey, R. T.; Cruickshank, F. R.; Pavlides, P.; Pugh, D.; Sherwood, J. N. *J. Phys. D: Appl. Phys.* **1991**, *24*, 135–145.
- (2) Tam, W.; Eaton, D. F.; Calabrese, J. C.; Williams, I. D.; Wang, Y.; Anderson, A. G. *Chem. Mater.* **1989**, *1*, 128–140.
- (3) Lagadic, I.; Lacroix, P. G.; Clément, R. *Chem. Mater.* **1997**, *9*, 2004–2012.
- (4) Lacroix, P. G.; Clément, R.; Nakatani, K.; Zyss, J.; Ledoux, I. *Science* **1994**, *263*, 658–660.
- (5) Mitzi, D. B. *Prog. Inorg. Chem.* **1999**, *48*, 1–121.
- (6) Whittingham, M. S.; Jacobson, A. J. *Intercalation Chemistry*; Academic Press: New York, 1982.
- (7) Chen, X.; Yang, C.; Qin, J.; Yakushi, K.; Nakazama, Y.; Ichimura, K. *J. Solid State Chem.* **2000**, *150*, 258–265.
- (8) Kauzlarich, S. M.; Stanton, J. L.; Faber, J. J.; Averill, B. A. *J. Am. Chem. Soc.* **1986**, *108*, 7946–7951.
- (9) Kargin, I.; Richeson, D. *Chem. Mater.* **1996**, *8*, 480–485.
- (10) Whittingham, M. S. *Prog. Solid St. Chem.* **1978**, *12*, 41–99.
- (11) Heising, J.; Bonhomme, F.; Kanatzidis, M. G. *J. Solid State Chem.* **1998**, *139*, 22–26.
- (12) Wang, L.; Schindler, J.; Thomas, J. A.; Kannewurf, C. R.; Kanatzidis, M. G. *Chem. Mater.* **2000**, *7*, 1753–1755.
- (13) Ke, S.; Ying, M.; Ya-an, C.; Zhao-hui, C.; Xue-hai, J.; Jian-nian, Y. *Chem. Mater.* **2001**, *13*, 250–252.
- (14) Choy, J.-H.; Kim, Y.-I.; Kim, B.-W.; Park, N.-G.; Campet, G.; Grenier, J.-C. *Chem. Mater.* **2000**, *12*, 2950–2956.
- (15) Py, M. A.; Haering, R. R. *Can. J. Phys.* **1983**, *61*, 76–84.
- (16) Clément, R.; Girerd, J. J.; Morgenstern-Badarau, I. *Inorg. Chem.* **1980**, *19*, 2852–2854.
- (17) Léautistic, A.; Rivière, E.; Clément, R. *J. Phys. Chem. B* **1999**, *103*, 4833–4838.

(18) Kim, J.; Wang, C.; Hughbanks, T. *Inorg. Chem.* **1998**, *37*, 1428–1429.

(19) Kim, J.; Wang, C.; Hughbanks, T. *Inorg. Chem.* **1999**, *38*, 235–242.

(20) Huheey, J. E.; Keiter, E. A.; Keiter, R. L. *Inorganic Chemistry: Principles of Structure and Reactivity*, 4th ed.; Harper Collins: New York, 1993.

(21) Pauling, L. *The Nature of the Chemical Bond*, 3rd ed.; Cornell University Press: Ithaca, NY, 1960.

(22) Pouchert, C. J. *The Aldrich Library of Infrared Spectra*, 3rd ed.; Aldrich Chemical Co.: Milwaukee, WI, 1981.

responsible for $\approx 91.3\%$ (w/w) of the reaction product with no detectable Li. Neutron activation analyses (Kaman Sciences, Model A71; detector: Ortec Germanium γ -ray Detector) showed N:Mn = 0.89(5):1 (molar), consistent with a $(\text{CH}_3\text{NH}_3)\text{MnTe}_2$ (yield $\approx 89\%$) composition and MnTe_2 content of $\approx 11\%$. Thermogravimetric analysis (TGA, Shimadzu TGA-50) showed a 9.6% weight loss when the product was heated to $550\text{ }^\circ\text{C}$, in reasonable agreement with an organic content of 8.7% (from AA).

Step-scanned X-ray powder diffraction data were collected by use of a Rigaku computer-automated diffractometer (RU200R) between 5° and 85° in 2θ with a step size of 0.02° and 6 s/step count time. The cell parameters, X-ray powder pattern, and the Mn/Te composition suggested that the new phase is isostructural with AMnTe_2 ($\text{A} = \text{K, Rb, Cs}$), from which starting metrical and thermal parameters were derived for the refinement.¹⁹ During Rietveld refinement, Mn and Te thermal parameters were constrained to 0.025, based on corresponding values from KMnTe_2 .²³ The refinement produced a converged Te position that yields an Mn–Te distance close to that in isostructural AMnTe_2 ($\text{A} = \text{K, Rb, Cs}$)²⁴ and a MnTe_2 fraction of 14%, comparable to the result from elemental analysis (11%). Attempts to locate CH_3NH_3^+ ions between $[\text{MnTe}_2^-]$ layers were fruitless. The presence of CH_3NH_3^+ in the refinement did not significantly affect the residual value or the refined Te position.

To shed light on the positioning and orientations of CH_3NH_3^+ ions, molecular mechanics calculations were performed using the *Open Force Field* (OFF) program in the *Cerius²* package (version 4.2).²⁵ This method has been employed to model small organic molecules intercalated between rigid host layers.^{26–28} Partial atomic charges for CH_3NH_3^+ and $[\text{MnTe}_2^-]$ layers were calculated by use of the *Charge-Equilibration* (Qeq) program in *Cerius²*.²⁹ Optimizations were carried out by minimizing the sum of van der Waals and Coulombic energies over a $(2a \times 2a)$ superlattice using *Universal Force Field* (UFF, version 1.02) as implemented in *Cerius²*.³⁰ Two initial models were constructed with different alignments of CH_3NH_3^+ molecules between $[\text{MnTe}_2^-]$ layers; the layer structures were constrained to conform with results from Rietveld refinement. The first model had all C–N bonds pointing “up” (parallel to *c* axis), and in the second model C–N vectors alternated “up” and “down”, giving rise to net zero dipole moment. In both models, the C–N midpoint was initially located in the (0.0 0.0 0.0) and (0.5 0.5 0.5) positions (occupied by alkali metals in $(\text{K, Rb, Cs})\text{MnTe}_2$). During the optimization, cell parameters, interlayer

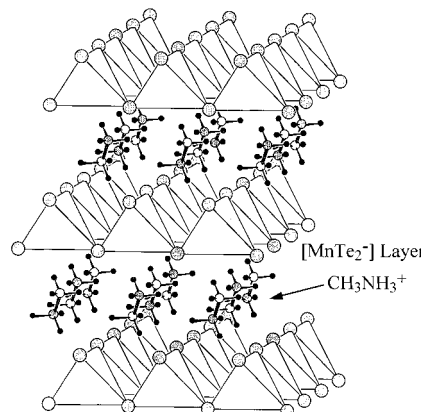


Figure 1. Proposed $(\text{CH}_3\text{NH}_3)\text{MnTe}_2$ structure.

spacing, and the positions of $[\text{MnTe}_2]$ layers were constrained, while the positions of CH_3NH_3^+ were allowed to move.

Figure 1 shows the proposed structure of $(\text{CH}_3\text{NH}_3)\text{MnTe}_2$ obtained from optimization of CH_3NH_3^+ positions and Rietveld refinement of $[\text{MnTe}_2]$ layers. In the optimized models, CH_3NH_3^+ molecules are oriented with C–N bonds tilted 15° from the *c* axis. The C–N bond midpoints remained close to (0.0 0.0 0.0) and (0.5 0.5 0.5). The second model (alternative C–N bond alignment) yielded lower energies than the first by 31.3 kJ/mol when the observed cell parameters were used. We performed the same optimization by varying the *c* axis from 16.029 to 18.029 Å in 0.25 Å increments for both models; the lowest energy was found at 16.779 Å in both models—reasonably close to the observed *c* axis (17.029 Å). The optimized energies at *c* = 16.779 Å were 6.99 kJ/mol (first model) and 8.91 kJ/mol (second model) less than that calculated at the observed *c* axis distance. The second model yielded lower energies than the first for all *c* axis lengths.

The ambient temperature rearrangement of $[\text{MnTe}_{3/3}]$ layers in LiMnTe_2 to the tetragonal $[\text{MnTe}_{4/2}]$ layers found in $(\text{CH}_3\text{NH}_3)\text{MnTe}_2$ is unprecedented. The same rearrangement occurs in syntheses of AMnTe_2 ($\text{A} = \text{K, Rb, Cs}$) when these compounds are prepared in reactions between LiMnTe_2 and $\text{A}_{0.5}\text{Li}_{0.5}\text{Cl}$ ($\text{A} = \text{K, Rb, Cs}$), but these reactions were carried out at greater than $600\text{ }^\circ\text{C}$.¹⁹ A conversion in the opposite sense is observed when $\text{AgAlS}_2\text{--I}$ is converted to $\text{AgAlS}_2\text{--II}$ at $350\text{ }^\circ\text{C}$ and 25 kbar.³¹

Since the layer rearrangement involves changes in the Te coordination number with respect to Mn, cleavage and formation of Mn–Te bonds is necessary. We speculate that the formation of molecular ionic species is involved and that such species are present in a low steady-state concentration throughout the reaction. The formation of the byproduct, MnTe_2 , is the formal result of oxidation (Te^{2-} to $1/2\text{Te}_2^{2-}$) and reduction (Mn^{III} to Mn^{II}) of dissolved ionic species. Related to this is the formation of MnTe_2 by the reaction of ammonium chloride and LiMnTe_2 in methanol. After 3 days' stirring, the reaction mixture color changes from brown to black. Gases are visibly evolved, and upon opening of the ampule under nitrogen, NH_3 was readily detected.

(23) Rietveld, H. M. *J. Appl. Crystallogr.* **1969**, *2*, 65–71.
 (24) *fw* = 342.21, space group $\bar{I}4m2$, $Z = 2$, $T = 25\text{ }^\circ\text{C}$, $\lambda = 1.5406\text{ \AA}$, 7703 data points, 4 variables, $R_p = 11.83\%$, $R_{wp} = 14.62\%$, $\chi^2 = 2.91$, $S = 1.708$.
 (25) *Cerius²*; Molecular Simulation Inc.: San Diego, CA, June 2000.
 (26) Yu, J.; Li, J.; Wang, K.; Xu, R.; Sugiyama, K.; Terasaki, O. *Chem. Mater.* **2000**, *12*, 3783–3787.
 (27) Capková, P.; Walter, J. *J. Solid State Chem.* **2000**, *149*, 68–74.
 (28) Capková, P.; Trchová, M.; Zima, V.; Schenk, H. *J. Solid State Chem.* **2000**, *150*, 356–362.
 (29) Rappe, A. K.; Goddard, W. A., III. *J. Phys. Chem.* **1991**, *95*, 3358–3363.
 (30) Rappe, A. K.; Casewit, C. J.; Colwell, K. S.; Goddard, W. A., III; Skiff, W. M. *J. Am. Chem. Soc.* **1992**, *114*, 10024–10035.

(31) Range, K.; Engert, G.; Weiss, A. *Z. Naturforsch.* **1974**, *29b*, 186–189.

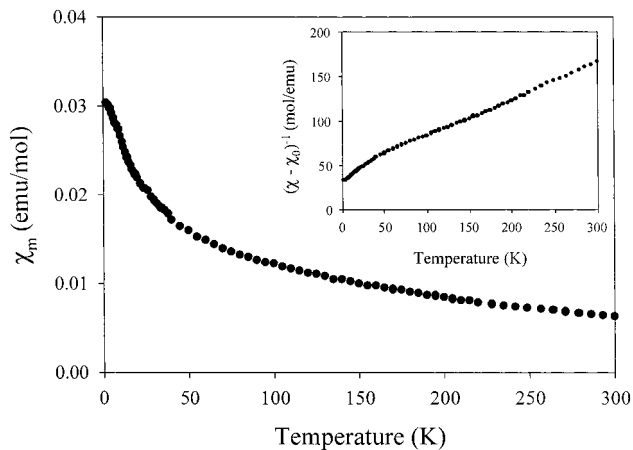
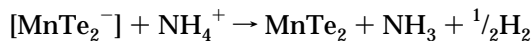


Figure 2. Temperature-dependent molar magnetic susceptibility (χ) for $(\text{CH}_3\text{NH}_3)\text{MnTe}_2$. χ^{-1} is shown in the inset.

X-ray powder diffraction data confirms that the black product is MnTe_2 ; the net reaction is presumed to be



Mn^{III} in LiMnTe_2 and protons in ammonium cation are reduced while tellurides (Te^{2-}) are oxidized to form $\text{Te}-\text{Te}$ bonds in MnTe_2 .

Temperature-dependent magnetic susceptibility data for $(\text{CH}_3\text{NH}_3)\text{MnTe}_2$ were measured (Quantum Design, Model MPMS XL) over the temperature range 4–300 K. As the product contains $\approx 11\%$ of MnTe_2 , corrections were made correspondingly and results are shown in Figure 2. Data for $T > 50$ K were fit to a modified Curie–Weiss expression ($\chi = \chi_0 + C/(T - \theta)$), where χ_0 accounts for the temperature-independent contributions

commonly observed in the layered ternary manganese chalcogenides;^{19,32} $\chi_0 = 3.252 \times 10^{-3}$ emu/mol, $\theta = -120$ K, and $C = 2.606$ emu·K/mol. The effective magnetic moment, μ_{eff} ($= 2.828 C^{1/2}$) was $4.57 \mu_{\text{B}}$, close to $4.90 \mu_{\text{B}}$ ($S = 2$) expected for high-spin Mn^{III} comparable to the results for AMnTe_2 ($\text{A} = \text{K, Rb, Cs}$).¹⁹ The negative Weiss temperature ($\theta = -120$ K) is indicative of strong antiferromagnetic interactions, but it seems that three-dimensional ordering does not occur.

Acknowledgment. Generous support was provided by the TARP through Grant 010366-0038b-1997 and the NSF through Grant CHE-9623255. We thank Bradley Smucker, Dr. Renald Guillemette, Dr. Anatoly Bortun, Lindsay Roy, and Dr. W. Dennis James for their assistance with magnetic susceptibility measurements and various analyses (microprobe, AA, thermogravimetric, neutron activation). We are especially thankful to Dr. Lisa M. Thomson (Laboratory for Molecular Simulation at Texas A&M University) for assistance with molecular mechanics calculations. Computing equipment and the *Cerius²* suite of programs were purchased with NSF Grant CHE-9528196.

Supporting Information Available: Figures S1, S2, and S3 for observed and calculated X-ray powder pattern of product, X-ray powder pattern of MnTe_2 , and optimized energies of two models with different c axes (PDF). This material is available free of charge via the Internet at <http://pubs.acs.org>.

CM010548K

(32) Kim, J.; Hughbanks, T. *J. Solid State Chem.* **1999**, *145*, 217–225.